Mechanism of Electroinduced Ionic Species Transport through a Multilamellar Lipid System

Yuri A. Chizmadzhev,* Vladimir G. Zarnitsin,* James C. Weaver,‡ and Russell O. Potts§
*Frumkin Institute of Electrochemistry, Moscow V-71, Russia; ‡Harvard-MIT Division of Health Sciences and Technology, Massachusetts Institute of Technology, Cambridge, Massachusetts 02139 USA, §Cygnus Therapeutic Systems, Redwood City, California 94063 USA

ABSTRACT A theoretical model for electroporation of multilamellar lipid system due to a series of large electrical pulses is presented and then used to predict the functional dependence of the transport of charged molecules. Previously, electroporation has been considered only for single bilayer systems such as artificial planar bilayer membranes and cell membranes. The former have been extensively studied with respect to electrical and mechanical behavior, and the latter with respect to molecular transport. Recent experimental results for both molecular transport and electrical resistance changes in the stratum corneum (SC) suggest that electroporation also occurs in the multilamellar lipid membranes of the SC. In addition, there is the possibility that other skin structures (the "appendages") also experience electroporation. A compartment model is introduced to describe the transport of charged species across the SC, and the predicted dependence is compared with available data. In this model, the SC is assumed to contain many hydrophilic compartments in series separated by boundary bilayers, so that these compartments become connected only upon electroporation. Two limiting cases for the transport of charged molecules are considered: (1) transport along tortuous inter-bilayer pathways in each compartment, followed by transport across individual boundary bilayers due to electroporation, and (2) transport along straight-through pathways in the boundary bilayers with fast mixing in each compartment, which includes the interior space of corneocytes. Both models were fitted to the experimental data. The large electropore radius ($r_t \sim 200$ Å) and porated fractional area ($f_t \sim 10^{-3}$) obtained from the fitting for the tortuous model relative to the more reasonable values obtained for the straight-through model ($r_s \sim 4$ Å, $f_s \sim 10^{-6}$) suggest that the latter is a more realistic description of electroinduced transport of ionized species through the skin.

NOTATIONS

A = $ze\tilde{E}/kT$
a_0 = area per lipid molecule
B = $zeE_{av}D/kT$
c = concentration
c_0 = concentration at $x = 0$
$c_{st}(x)$ = stationary concentration profile
D = diffusion coefficient
$\tilde{D}$ = $D(\ell/\tilde{h})$
d = bilayer thickness, ~50 Å
E = electric field strength
$\tilde{E}$ = E/β
E_{av} = time-averaged strength of electric field
e = absolute value of electric charge
f = a fractional area of all pathways
H = SC layer thickness, ~20 μm
$\tilde{H}$ = $H\beta$
h = distance between the cells in x direction, 0.05 μm
$\tilde{h}$ = the thickness of boundary layer between two compartments
J = average flux density per unit of apparent surface
J_{eff} = efflux density
J_{inf} = influx density
j = flux density through a single pathway
$\hat{j}$ = time-averaged flux
K_p = the rate of hydrophilic pore formation
k = Boltzman constant
L = corneocyte length, ~30 μm
ℓ = corneocyte thickness, ~1 μm
N = pore density
n = the number of lipid bilayers in SC (in sequence)
n_c = the number of corneocytes in SC (in sequence)
R_b = the resistance of the surrounding solution
R_c = the resistance of the compartment interior
R_ℓ = the voltage-dependent resistance of the boundary lipid bilayers
R_s = the resistance of SC, ~10^5 ohms cm^2 in normal condition
R_x = the resistance of the main pathway for small ions (e.g., Na^+, Cl^-)
r = pore radius
r_* = pore radius at the transition point from hydrophilic to hydrophobic state
r_s = pore radius in the straight-through model
r_t = pore radius in the tortuous model
S = area of the membrane
T = absolute temperature, K
t = time
$\tilde{t}$ = renormalized time
t_d = diffusional relaxation time
t_f = time of electrotreatment
t_{fr} = front movement time
t_i = interpulse pause
t_m = migrational relaxation time
t_p = pulse duration
U = outer voltage drop
U_ℓ = voltage drop on R_ℓ
U_s = voltage drop on the layer of SC
U^* = eU_s/kT
v = velocity of front movement
x = coordinate
$\tilde{x}$ = βx renormalized distance
z = charge number

Received for publication 14 April 1994 and in final form 7 November 1994.
Address reprint requests to Dr. Russell O. Potts, Cygnus Therapeutic Systems, 400 Penobscot Drive, Redwood City, CA 94063. Tel.: 415-369-4300; Fax: 415-369-5318.

0006-3495/95/03/749/17 $2.00

α $\pi r_*^2(\epsilon_w - \epsilon_m)\epsilon_0/2dkTn^2$
β = tortuosity of the pathway
Γ = partition coefficient
γ = the accessible fraction of the compartments volume
Δ = the thickness of epidermis
ΔW = activation energy of hydrophilic pore formation
ΔW^0 = activation energy of hydrophilic pore formation at ($u = 0$)
δ = inter-bilayer thickness, 5–10 Å
ν = frequency of lateral fluctuations of lipid molecule
ϵ_m = dielectric permittivity of membrane
ϵ_w = dielectric permittivity of water
ϵ_0 = dielectric constant of vacuum
ρ = the specific resistance of the electrolyte solution

INTRODUCTION

Drug delivery through the skin has a number of potential advantages relative to other means of administration, including the reduction of enzymatic drug degradation and the ability to establish uniform (steady) drug delivery. The difficulty with transdermal drug delivery is that the skin is a formidable barrier that significantly reduces the transport of extraneous substances, especially large, ionized molecules. Many therapeutically useful substances have high molecular weights and are hydrophilic or ionized. It is important, therefore, to permeabilize the skin transiently and reversibly to achieve therapeutic transdermal drug delivery. A similar problem of drug uptake by cells in suspension has been addressed by electrical treatment with short pulses of a strong electric field. It was shown that cell permeabilization is a consequence of the electroporation of plasma membranes, which results in the creation of new pathways through the lipid bilayer. This phenomenon has been widely studied in a variety of lipid bilayers and cell membranes (Neumann and Rosenheck, 1972; Kinosita and Tsong, 1977; Abidor et al., 1979; Tsong, 1991; Weaver, 1992; Weaver, 1993). Electroporation is now used in many therapeutic applications: drug delivery into cells and liposomes, including uptake of large molecules such as DNA, and the insertion of membrane proteins in cell membranes (for references, see Neumann et al., 1979; Chang et al., 1992). In addition, anti-tumor drug delivery (Mir et al., 1991; Orlowski and Mir, 1993) and in vivo electrotransformation (Titomirov et al., 1991) are two promising therapeutic applications. It has been suggested that transport in all cases is through transient pores in the lipid membrane produced by the electric field. It is important to mention that the electric field plays a double role by causing pore formation and by acting as a driving force during electrophoresis (Xie and Tsong, 1990; Klenchin et al., 1991; Sukharev et al., 1992).

Utilization of an electric field in transdermal delivery is not new. Iontophoresis, which was described many years ago (for references, see Burnette, 1989). Increased drug delivery in this case is because electromigration is more effective than passive diffusion. In the range of small applied voltages ($U < 1$ V), where all effects are linear with the field, there is no evidence to suggest the creation of new pathways (Dinh et al., 1993). From direct measurements (Cullander and Guy, 1991; Scott et al., 1993), it has been determined that the primary iontophoretic pathway for small ions is associated with skin appendages (e.g., sweat glands and hair follicles) (see Fig. 1). At the same time, it is not possible to exclude transport through preexisting pathways within the lipid lamellae-corneocytes region of the stratum corneum (SC), especially for small ions (Grimnes, 1983; Monteiro-Riviere et al., 1994). In any case, it is clear that at a potential difference of less than 1 V, the electric field provides only a driving force for ion migration, not for the creation of a new pathway. The situation, however, changes drastically with increasing voltage. For example, at a potential of a few volts (Kasting and Bowman, 1990a, b), the current-voltage behavior of human skin becomes nonlinear. Under these conditions, a steady-state potential develops with significant lag time, and the system acquires some features of irreversibility. This behavior is contrary to classical electrodiffusion theory, leading to a description of this nonohmic behavior in terms of either interfacial limiting stages or electroporation (Kasting and Bowman, 1990a, b). No distinction between these two hypotheses was discussed, however, even though only the latter can explain irreversibility. Also, in these descriptions of nonohmic behavior, there is no discussion of the site of electroporation, although it seems likely that if the applied potential (U) is about 1 V,[1] only a few layers of the cells could be porated. This suggests that skin appendages are primarily involved and that electroporation could take place at the level of the epithelial cells that line the appendages. Moreover, for $U \sim 1$ V, it is unlikely that electroporation occurs in the SC, because there are on order of 100 lipid bilayers in a series, resulting in a voltage drop of about 10 mV on each. Indeed, this value is significantly smaller than the typical "threshold voltage" for lipid bilayer electroporation.[2] However, when the voltage applied across the skin (U_s) is increased to about 50 V, the situation changes dramatically. As shown in Prausnitz et al. (1993), after the treatment of human skin in vitro by a sequence of high-voltage, short duration pulses, the flux of calcein increased by several orders of magnitude. Similar results were obtained for the electroporative transport of metoprolol through rat skin (Vanbever et al., 1994). In addition, even a single, high voltage pulse is sufficient to increase significantly the iontophoretic transport of peptides through human skin in vitro (Bommannan et al., 1993, 1994). There is reason to believe, therefore, that these results are due to the creation of new pathways in the SC under the influence of an electric field, because in this case, the voltage drop across a single bilayer is sufficient for electroporation. At the same time, the

[1] Here, U is the applied voltage across the solution and skin. The skin's resistance (measured in the presence of small ions such as Na^+ and Cl^-) before electroporation ($\sim 10^5$ ohms cm^2) is much larger than that of the bathing solution ($\sim 10^2$ ohms cm^2). As a consequence, most of the voltage drop occurs across the skin. After electroporation, the skin and solution resistance are of the same order of magnitude.

[2] Strictly speaking, "threshold voltage" is a conditional notion because it depends on the pulse duration.

activation of the usual iontophoretic pathways through skin appendages cannot explain this effect due to the saturation of the membrane potential (Benz et al., 1979; Kinosita et al., 1988) and a voltage divider effect (Weaver and Barnett, 1992). It is possible, however, that enhanced permeability results from electrically induced deformation of sweat glands (Edelberg, 1971). The consideration of this latter mechanism is beyond the scope of this paper, where we describe a quantitative analyses of ionized drug delivery through the skin due to electroporation of SC.

STRUCTURAL MODEL OF STRATUM CORNEUM

Mammalian skin (Fig. 1) is comprised of two layers, the epidermis and the dermis. The dermis consists of connective tissue and contains appendages such as hair follicles and sweat glands, which extend upward to the surface. In addition, the dermis is vascularized, with a high density of capillar loops just below the dermal-epidermal junction. The dermis and epidermis (without SC) have a high water permeability. The epidermis is avascular and extends about 100 μm below the skin's surface. The outer layer of the skin, the SC, constitutes the main barrier to the transport of ionized molecules (Potts and Guy, 1992; Odland, 1983; Cullander, 1992; Michaels et al., 1975; Elias, 1983). The SC has a thickness of about 10–20 μm and consists of about 20 layers of flattened keratin-filled cells (corneocytes) surrounded by lipid lamellae containing cholesterol, free fatty acids, and ceramides (Potts, 1989; Madison et al., 1987). Finally, the entire epidermis is crossed by appendages that are characterized by relative cross section area of about 0.1%.

According to electron micrographs and other data (Madison et al., 1987; Holbrook and Odland, 1974; Swartzendruber et al., 1989; Elias et al., 1977), the lipid domain of the SC surrounds and separates the corneocytes. A schematic diagram of the SC is shown in Fig. 2 *a*, where the discrete shaded areas represent the corneocytes and the continuous, clear areas represent the lipid domain. Between each corneocyte, there are several lipid bilayers, each with a

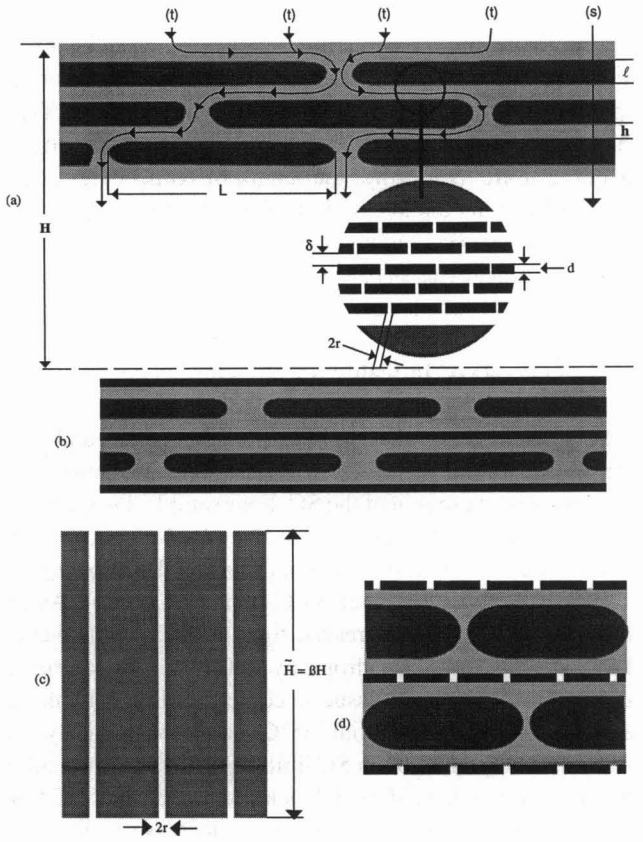

FIGURE 2 Structural and transport models of SC. (*a*) A schematic representation of human SC where the corneocytes are shown by the shaded area and are surrounded by the lipid domain. The lipid and lipid-corneocyte routes of ion transport are designated as t and s, respectively. The inset shows the multi-lammelar lipid domain after formation of electropores (for details, see text). (*b*) A schematic model of the SC comprised of discrete layers of corneocytes isolated by multilamellar lipids. The corneocytes are shown by the shaded area. The lipids that isolate each compartment are shown by the thick solid line. (*c*) The equivalent pathway representation of the lipid (tortuous) route, shown as t in *a*. (*d*) A schematic representation of reservoir (straight-through) model with electropores induced in SC lipids separating the compartments.

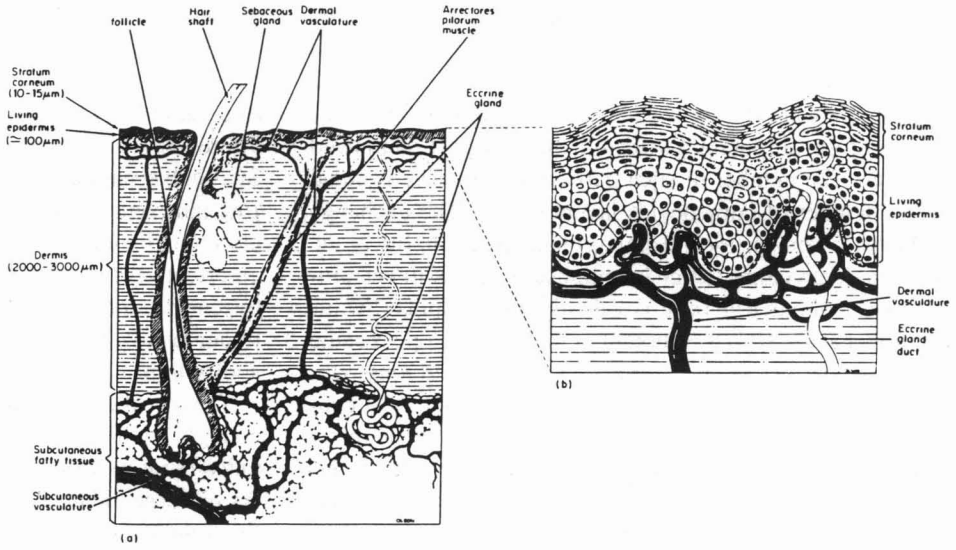

FIGURE 1 A schematic representation of the structure of human skin.

hydrophilic core of thickness of about 30–40 Å and the inter-bilayer (hydrophilic) domain of about 15–25 Å thickness (Potts, 1989; Bouwstra, 1992). A detailed structure of the lipid domain after electroporation is shown in the inset. Typical values for the structural parameters of the SC illustrated in Fig. 2 *a* are as follows: the length of corneocytes (L) is about 30 μm, its thickness (ℓ) is about 1 μm, the thickness of the SC layer (H) is about 20 μm, and the distance between adjacent corneocytes (h) is about 0.05 μm. The inter-bilayer thickness (δ), which is accessible for hydrophilic transport is estimated to be about 5–10 Å, whereas the bilayer thickness (d) is about 50 Å. In reality, the structure is not as regular as shown in Fig. 2 *a*.

It is very unlikely that there is an appreciable number of preexisting, continuous hydrophilic pathways across the lipid-corneocyte region of the SC. For example, the electrical resistance of human skin as determined by Na^+ and Cl^- ion conductance is very high and remains around 100 kohm cm^2 at temperatures up to about 60°C (Oh et al., 1993). As the temperature is further increased from 60 to 70°C, however, the skin resistance (R_s) drops by 100-fold, but returns to initial values when the tissue is cooled. This reversible resistance transition at about 65°C parallels precisely the chain-melting transition in SC lipids. Similarly, treatment of the skin with oleic acid, which is known to disrupt SC lipid structure, also resulted in a dramatic decrease in R_s (Potts et al., 1992). At low temperatures, small ion transport occurs primarily via appendageal route. As the SC lipid structure is disrupted, however, either by increasing the temperature or by the addition of a lipid perturbing compound, ion transport occurs via both the appendageal and lipid-corneocyte routes.

For the purposes of transport, we propose the model of the SC as a sequence of discrete compartments in series, each containing one layer of corneocytes and the intervening lipid lamellae (Fig. 2 *b*). The hydrophilic space of each compartment consists of an accessible (or free) volume of the corneocyte, as well as the inter-bilayer space between the polar head groups of the lipid lamellae. As a consequence of the continuous, hydrophilic space in each compartment, there is a redistribution of ionized particles within each. At the same time, each compartment is isolated from those above and below by a few lipid bilayers oriented parallel to the SC surface. They are shown as dark thick lines in Fig. 2 *b*. Thus, bilayers form the main barrier for the transport of ionized particles. The number of such barriers in sequence is equal to the number of corneocytes layers (~20). The exchange within each compartment depends on the permeability of the corneocyte envelope, which is composed of cross-linked proteins with an outer layer of covalently bound lipids (Swartzendruber et al., 1987). Although rigid, this envelope is at the same time permeable to water and probably small ions. Water in the SC is found mainly within the corneocytes at concentrations up to 1 g water per 1 g of dry tissue (Scheuplein and Bronaugh, 1983). Little is known currently about permeability of the corneocyte envelope to large charged particles or its ability to be electroporated.

With this background in mind, we propose three potential pathways for the transport of hydrophilic substances through the epidermis: the hair follicles and other existing hydrophilic pores (the appendageal route), the lipid lamellae of SC, bypassing corneocytes (the lipid-tortuous route, designated t in Fig. 2 *a*), and both the corneocytes and lipid bilayers (the lipid-corneocyte straight-through route, designated s in Fig. 2 *a*).

In the case of iontophoresis, for which the applied potential is less than a few volts, the primary preexisting pathway is most likely via the appendageal route (Cullander, 1992; Scott et al., 1993). At the same time, it is difficult to exclude participation of lipid and lipid-corneocyte routes because of the possible existence of structural defects within the SC lipids (Grimnes, 1983; Cullander, 1992; Potts et al., 1992). When the applied voltage is large enough to electroporate the SC lipid lamellae, however, other pathways could, in principle, appear and predominate. It is well known (for references see review by Tsong (1991) that under electrical perturbation, pores are formed in other lipid bilayers. A similar phenomenon may occur in SC lipid bilayers, resulting in the formation of pores in the lipid barriers between compartments and thereby providing a new continuous hydrophilic route across all SC layers. It is interesting to note that this effect of the electric field is similar to the chain-melting in SC lipids or the disruption of SC lipid structure by oleic acid, both known to enhance transport through the SC.

It is important to describe the range of the voltage where significant poration of SC lipids can be induced. From an electrostatic point of view, the SC can be considered a dielectric with a high leakage resistance of ($\geq 10^5$ ohms cm^2) and a specific capacitance about 0.03 μF/cm^2 (Oh et al., 1993; Edelberg, 1971). If the SC is considered a homogeneous medium of 20 μm thickness, an average dielectric permittivity (ϵ) of 700 is obtained. This value of ϵ is unreasonable, suggesting that the homogeneous model of the SC is not valid (DeNuzzio and Berner, 1990). Alternatively, we should take into account the fact that corneocytes contain water and small ions resulting in an equipotential domain within these compartments. Thus, the potential drop across the SC may occur predominantly across the lipid domain between the corneocytes. This lipid domain can be described as parallel resistors and capacitors in series through the SC. There are on average about 20 corneocyte layers in the SC, each separated by lipid domain of thickness about 0.05 μm and containing on the order of five bilayers. Thus, the effective thickness is about 1 μm (20 $\times$ 0.05 μm), yielding an effective dielectric permittivity of about 20, a value between that for pure lipids (~3) and water (~80). This estimation suggests that the voltage drop is concentrated only across lipid bilayers that are oriented normal to the field.

The so called "threshold" potential for electroporation on a single lipid membrane is about 0.5–1 V and depends on pulse duration (for references see review by Tsong (1991). As discussed above, there are on the order of 100 bilayers throughout the thickness of the SC. This means that a voltage

on SC of about 50–100 V should be sufficient to cause electroporation and concomitant increase in flux. This is an order of magnitude estimation because there are no data on the electroporation property of SC and its components. Nevertheless, this calculation suggests that SC electroporation occurs at voltages of about 50–100 V, consistent with experimental results (Prausnitz et al., 1993; Bommannan et al., 1993; Vanbever et al., 1994, Bommannan et al., 1994).

A compartment model of SC is rather general and can be used to describe the transport of large, ionized molecules through lipid and lipid-corneocyte routes. To simplify the calculations, we have considered two limiting transport mechanisms. In one, the corneocyte envelopes are considered impermeable to large ions, and transport within each compartment is entirely along hydrophilic inter-bilayer domains. This rate is assumed to be slow compared with the charge transfer rate across electropores induced in the boundary lipid bilayers. This tortuous (lipid) route is shown schematically in Fig. 2 *a* (designated t). In the other extreme, the redistribution of ionized particles within the hydrophilic compartment is assumed to be fast, and the slow stage is attributed to the penetration through induced electropores. This straight-through (lipid-corneocyte) route is shown schematically in Fig. 2 *a* (designated s). This model includes the possibility of reservoirs for large, ionized molecules in either the hydrophilic domain between lipid bilayers (if corneocyte envelopes are assumed to be impermeable) or within the intercellular space of corneocytes. The difference between these two cases is manifested only in the free volume of the ion reservoir, which is much larger in the second case.

ELECTROPORATION OF SC LIPID BILAYERS

In both models, continuous transport pathways are induced as a result of electroporation of lipid bilayers forming the boundaries between the compartments. Assuming that electroporation is reversible, the energy profile of the pore has the form shown in Fig. 3 (Glaser et al., 1988). The energy described by branch 1 corresponds to the hydrophobic pore, and branch 2 to the hydrophilic pore. Only hydrophilic pores participate in ion transport. Under the influence of an electric field, the potential energy decreases (Fig. 3) and, as a consequence, the density $N(t)$ of hydrophilic pores increases. If the duration of the pulse is sufficiently long or the amplitude is sufficiently high, the probability of the hydrophilic pore overcoming the second energy barrier also increases, resulting in an irreversible breakdown of the lipid bilayer. In therapeutic applications, it is important to avoid such effects. In the experiments utilizing human skin (Prausnitz et al., 1993), especially in the case of high amplitude pulses, partial irreversibility of electroporation was observed. For this reason, in the course of the fitting of the theory with experimental data (see Fitting of the Experimental Data to Theoretical Models), the level of residual permeability will be introduced formally as boundary condition at $t \to \infty$.

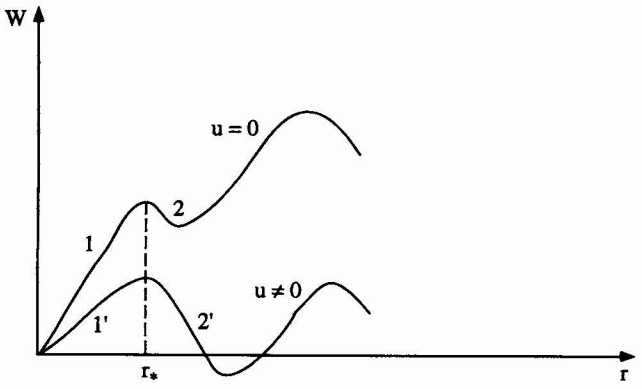

FIGURE 3 The energy profile of the pore. Curve 1 corresponds to the energy of hydrophobic pore, curve 2 to the energy of hydrophilic pore; curve 2′ corresponds to the energy profile of the pore during electrical treatment. u, voltage drop on single bilayer; r^*, the radius of the pore in activated state.

The rate (K_p) of hydrophilic pore formation can be calculated (Glaser et al., 1988)

$$K_p = \frac{S\nu}{a} \exp\left(-\frac{\Delta W}{kT}\right), \tag{1}$$

where a is the area occupied by a single lipid molecule, ν is the frequency of lateral fluctuations of lipid molecules, k is the Boltzman constant, T is the absolute temperature, and S is the membrane area. The activation energy is

$$\Delta W = \Delta W^0 - \frac{\pi r_*^2(\epsilon_w - \epsilon_m)\epsilon_0 u^2}{2d}, \tag{2}$$

where ΔW^0 is the activation energy in the case $u = 0$, u is a potential difference across a single bilayer, ϵ_w is the relative permittivity of water inside the pore, ϵ_m is the relative permittivity of bilayer, ϵ_0 is the dielectric constant, and r_* is the radius in the activated state. We assume that the probability of pore formation is the same for any bilayer in the SC. In the numerical calculations presented here, the following experimental protocol (Prausnitz et al., 1993) will be used: pulse duration $t_p = 10^{-3}$ s, interpulse interval $t_i = 5$ s, total time of electrotreatment $t_f = 1$ h, pulse amplitude (U) was varied from 150–1000 V. The pore density $N(t)$ for the pulsed periodic protocol can be approximated by the equation

$$\frac{dN}{dt} = \frac{\nu}{a}\left[\frac{t_p}{t_i}\right] \exp\left[-\frac{\Delta W^0}{kT} + \frac{\pi r_*^2(\epsilon_w - \epsilon_m)\epsilon_0 u^2}{2dkT}\right] - \frac{N}{t_r}, \tag{3}$$

where t_r is the pore resealing time.

The voltage drop on a single bilayer (u) depends in general on U, the pore density N, and other electrical parameters of the system. To simplify this problem, we introduce an equivalent electrical circuit (Fig. 4) where, consistent with the experimental protocol (Prausnitz et al., 1993), the outer voltage U is maintained while the voltage U_s across the skin is measured. In this model, R_b represents the resistance of surrounding solution, and R_x corresponds to the main pathway for small ion transport (e.g., Na^+, Cl^-) through the skin. It includes appendages and other possible pathways in the SC

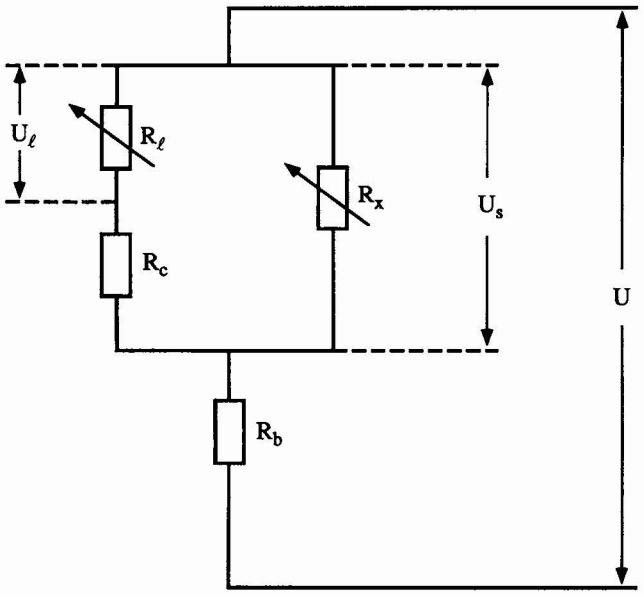

FIGURE 4 The equivalent electrical scheme of SC. The resistance of bulk solution R_b is in sequence with the skin resistance, which includes two parallel branches. The resistance R_x refers to the main pathways of background electrolyte (for example, NaCl) going through the appendages and stratum corneum. The resistance R_c corresponds to the inner part of each compartment and R_ℓ to lipid bilayers, forming boundaries between the compartments. U_s and U_ℓ are the voltage drop on the corresponding resistances.

accessible to small ions only. It was shown from tissue impedance measurements that over the range of voltages studied (U from about 100 to 1000 V), the skin resistance is much smaller ($R_s \sim 10^2$ ohms cm^2) compared with $R_s(U = 0) \sim 10^5$ ohms cm^2. This drop of the resistance occurs abruptly in a μs time interval after the application of voltage. Over the range of 0–100 V, R_x is strongly voltage-dependent, consistent with the results obtained by others (Kasting and Bowman, 1990a, b; D. Bommannan, unpublished data). In contrast, R_x changes little from 100 to 1000 V. It should be emphasized, however, that calcein flux showed a rather different voltage dependence. In particular, the calcein flux increased by several orders of magnitude in the range of 100 V < U < 300 V, but increased little with further increase in potential.

In parallel with R_x are two resistances in series within the lipid-corneocyte domain of the SC that correspond to an electrically induced pathway for both small (e.g., Na^+, Cl^-) and large ions (e.g., calcein). The two resistances found in this pathway are R_c, the voltage-independent resistance attributed to the compartment interior, and R_ℓ, the voltage-dependent resistance of the boundary lipid bilayers. This pathway is induced by an electric field where the calcein flux is increased by orders of magnitude when U was increased from 100 V up to about 300 V, but increased only slightly with further increases in potential.

The equivalent circuit contains two voltage dividers: one is between R_b and R_ℓ. If the resistance R_x becomes low ($R_x \ll R_x + R_\ell$), then the potential drop on the skin (U_s) is defined primarily by R_x. At low potential ($R_\ell \gg R_c$), little ion transport occurs via this pathway. At higher potential, however, electroporation reduces R_ℓ and the flux becomes limited by R_c. The voltage across R_ℓ is responsible for the voltage-dependent changes in calcein flux.

The voltage drop U_ℓ on the resistance R_ℓ is defined by

$$U_l = \frac{U_s}{1 + R_c/R_\ell}. \tag{4}$$

Taking into account that R_ℓ is inversely proportional to the number of pores ($R_\ell = R_\ell^0$, where R_ℓ^0 is a constant), and $U_\ell = un$, where n is the number of lipid bilayers in sequence, forming the barriers between compartments, the substitution of Eq. 4 into Eq. 3 yields

$$\frac{dN}{dt} = A \exp\left(\frac{\alpha \cdot U_s^2}{\{1 + R_c N/R_\ell^0\}^2}\right) - \frac{N}{t_r}, \tag{5}$$

where

$$A = \frac{\nu}{a}\left[\frac{t_p}{t_i}\right]\exp\left[-\frac{\Delta W^0}{kT}\right],$$
$$\alpha = \frac{\pi r_*^2(\epsilon_w - \epsilon_m)\epsilon_0}{2dkTn^2}, \qquad R_1^0 = \frac{\rho n d}{\pi r^2}. \tag{6}$$

Here, ρ is the specific resistance of the electrolyte solution and r is the average pore radius. In steady state, we have

$$N = t_r A \exp\left(\frac{\alpha U_s^2}{\{1 + R_c N/R_\ell^0\}^2}\right). \tag{7}$$

It is rather simple to find the solution of the Eq. 7 for two limiting cases:

1. At small potential across the skin, i.e.,

$$\alpha U_s^2 \frac{R_c N}{R_\ell^0} \ll 1, \tag{8}$$

the pore density $[N(U_s)]$ is strongly dependent upon U_s:

$$N \approx t_r A \exp(\alpha U_s^2). \tag{9}$$

2. In the limit of large U_s, when N also becomes large (i.e., $N \gg R_1^0/R_c$), the asymptotic expression for $N(U_s)$ is gently sloping

$$N \sim U_s^* \ln^{-0.5} U_s^*, \qquad \text{where} \quad U_s^* = \frac{eU_s}{kT}. \tag{10}$$

For the fitting of this theory with experimental data over the entire range of potentials, Eq. 7 was solved numerically and the results are presented below. It is important to emphasize that the results for the potential distribution and pore density are independent of specific model (tortuous or straight-through) of transport.

TORTUOUS (LIPID) MODEL

From Fig. 2 *a*, it is obvious that the hydrophilic, inter-bilayer pathways (designated t in Fig. 2 *a*) are characterized by a high tortuosity ($\beta = L/2(\ell + h) \sim 15$) dictated by the

structure of the SC. From electron microscopy results (Swartzendruber et al., 1989), the roughness of the cell surface has been estimated to be about 3 so that the total tortuosity β should be about 50. As a consequence, the actual length of lipid pathways ($\tilde{H}$) is equal to about 50 times the SC thickness (H), which agrees with estimates made for skin transport (Potts and Francoeur, 1991; Potts and Guy, 1992). Similarly, the effective electric field ($\tilde{E} = E/\beta$) in the direction of ion movement will be reduced 50-fold compared with the applied field (E). The value of E is equal to U_s/H, where U_s is the voltage across the SC. In the tortuous (lipid) model, the electrodiffusion of large, ionized molecules along such pathways is considered to be the slow transport process.

Instead of nonhomogeneous pathways along the hydrophilic inter-bilayer domains and through electropores induced in lipid bilayers, let us consider an equivalent model. This model (Fig. 2 *c*) consists of a population of homogeneous hydrophilic pathways which cross the SC, each of which has the same effective cross section, length ($\tilde{H}$), and reduced electric field ($\tilde{E}$). The number of pathways and the flux depends critically on the electric field.

Concentration profile

To define the flux of large ionized particles in an excess of background electrolyte through a single pathway as a function of time during (and after) the electrotreatment of the SC, it is necessary to calculate the concentration profile under the defined boundary and initial conditions, taking into account the time-dependent variation of the electric field [$E(t)$]. In one dimension, the transport of a ionized particle can be described by the equation

$$\frac{\partial c}{\partial t} = D\frac{\partial^2 c}{\partial x^2} - v\frac{\partial c}{\partial x}, \tag{11}$$

where

$$v = zeD\tilde{E}/kT \quad \text{and} \quad \tilde{x} = x\beta. \tag{12}$$

Here, c is the concentration in inter-bilayer hydrophilic domain, D is the diffusion coefficient in the same domain, e is the elementary charge, and z is the charge number. The solution of this electrodiffusion Eq. 11 with different boundary conditions is well known (Lakshminarayanaiah, 1984). The uniqueness of the present case lies in the periodic character of the function $\tilde{E}(t)$, and the dependence of the number (or total cross section) of accessible pathways on $\tilde{E}$ and t.

Because the lipid lamellae phase of SC in the absence of an electric field can be considered to be nonpermeable for hydrophilic substances, the initial condition is $c(\tilde{x}, 0) = 0$. The boundary condition at the inlet side of the SC has the form $c(0, t) = c_0 = \Gamma c_b$, where Γ is the partition coefficient and c_b is the concentration in the external solution. There are several versions of the boundary conditions at the outlet side of SC: A) The problem can be considered in semi-infinite space with $c(\infty) = 0$ and the flux calculated at $\tilde{x} = \tilde{H}$ can be taken as some approximation. B) It is better to solve Eq. 3 in the interval $0 < \tilde{x} < \tilde{H}$ with boundary condition $c(\tilde{H}, t) = 0$; (e.g., "sink" conditions). This condition corresponds to the very high diffusional permeability of the unstirred layer at outlet side of SC. C) The most rigorous formulation of the boundary condition takes into account the diffusional permeability of an unstirred layer. In this case, we should solve simultaneously the electrodiffusion problem in the interval $0 < \tilde{x} < \tilde{H}$, and the diffusion problem at $\tilde{H} < \tilde{x} < \tilde{H} + \Delta$, where Δ can be estimated as a thickness of epidermis ($\sim$100 μm). At $\tilde{x} = \tilde{H}$ the concentration and the flux should be continuous and $c(\tilde{H} + \Delta) = 0$. The problems A) and B) have simple analytical solutions when $\tilde{E}$ = const. The problem C) has a rather complicated solution in the form of series, even in the case $\tilde{E}$ = const. As was shown by numerical calculations for the periodic electrotreatment considered here, all three versions give similar solutions for the flux at $\tilde{x} = \tilde{H}$. The concentration profiles at $0 < \tilde{x} < \tilde{H}$ for the versions B) and C) are also very similar and, for this reason, our discussion will be restricted to the case of "sink" condition (version B). Unfortunately, the solution for periodic treatment, even in the case of "sink" condition at $\tilde{x} = \tilde{H}$, can only be obtained numerically. Therefore, let us consider some approximations that allow insight into the main features of the evolution of the concentration profile.

The diffusion relaxation time t_d for a layer of effective length $\tilde{H}$ is equal to $\tilde{H}^2/D$, whereas electrical migration relaxation time t_m for the same layer is equal to $\tilde{H}/v$. The ratio of these characteristic times is kT/zeU_s. The large difference of these characteristic times when $U_s \gg kT/ze$, defines the main features of the transport process described here (electromigration is greater than diffusion). For example, during the pulse with U_s = 500 V, $t_d/t_m \sim 10^{-5}$. Introducing the average voltage during the electrotreatment protocol, $U_{s,av} = U_s t_p/t_i$, we obtain $U_{s,av} \sim 10^{-1}$ V and $t_d/t_m \sim 6 \times 10^{-2}$. This result means that not only during the pulse, but also on average (taking into account relatively long interpulse intervals), diffusion effects have only a small influence on the evolution of concentration profile.

In Appendix A, the case $\tilde{E}$ = const is considered for the semi-infinite boundary problem. This approach describes the dynamics of concentration profile during single pulse and, to some extent, the approximation of the average field.

The solution (A9) of Eq. 11 corresponds to a moving concentration front that is broadened because of diffusion. The front velocity is defined by Eq. 12. The shift of the front during single pulse can be estimated as $\Delta\tilde{x}_p = vt_p$.

During the pause between pulses when the field is zero, only diffusional broadening of the front takes place, without any shift due to electromigration. The time interval ($t_{\tilde{H}}$) needed for the front to reach the base of the SC ($\tilde{x} = \tilde{H}$) is

$$t_{\tilde{H}} = t_m\left[\frac{t_p + t_i}{t_p}\right], \tag{13}$$

whereas the broadening of the front at that moment of time is $D\tilde{x} \sim [Dt_{\tilde{H}}]^{1/2}$.

For the electrical transport of calcein in human skin considered above (Prausnitz et al., 1993), values of $t_{\tilde{H}} = 8$ min and $\Delta\tilde{x} = 200$ μm were obtained. The ratio $\Delta\tilde{x}/\tilde{H} = 0.2$ suggests that after the application of 100 pulses with $U_s = 500$ V, 80% of the SC attains the initial concentration c_0. In the case of "sink" boundary conditions and $\tilde{E} = \text{const}$ (see Appendix B), the concentration profile approaches a steady-state solution (B3) at long times ($t \gg t_m$). If the application of the periodic electrical pulses is maintained for a longer time, steady oscillations of the concentration profile in the neighborhood of the outlet side of SC will result. During the pulse, the concentration front will shift by $\Delta\tilde{x}_p$, which should be equal to about 10 μm. During the pause between pulses, diffusional broadening of the concentration front takes place by an amount $\sim[Dt_i]^{1/2}$. The corresponding computer calculations are shown in Fig. 5. The numerical method of Crank-Nickolson was used for the calculation (Pearson, 1988). This algorithm was programmed in Turbo Pascal 5.5 on an IBM PC 486 computer. It is clear from Fig. 5 that the oscillations affect the region near the outlet side of the SC (curves 7 and 8). The width of this region is about 20 μm. It should be mentioned that all of these estimates were made in the coordinate system that corresponds to the equivalent pathway with a length $\tilde{H} = 1000$ μm. Thus, oscillations of the concentration profile will lead to a periodic behavior of the flux with characteristic frequency $2\pi/t_i$.

Flux density

The flux density trough a single pathway (j) can be described at either the inlet or the outlet surface of the SC. Instantaneous values of the flux are oscillatory functions of time and correspond to the periodic protocol of electrotreatment, differing at inlet and outlet sides of SC. The average flux, however, must be the same for both sides of the SC.

To calculate average flux at the inlet side, we should take into account that near the SC surface ($\tilde{x} = 0$) the concentration is practically constant and equals c_0. This means that only electromigration determines the flux at this side, because there is no concentration gradient to drive diffusion. Hence, the average flux $\bar{j}_0$ at the SC surface ($\tilde{x} = 0$) is

$$\bar{j}_o = \frac{1}{t_p + t_i}\int_0^{t_p + t_i} j_o(t)\,dt = \frac{c_0 v t_p}{t_p + t_i}, \qquad (14)$$

where the subscript o refers to the corresponding quantity at the surface ($\tilde{x} = 0$), and $j_0(t)$ is the instantaneous value at $\tilde{x} = 0$.

The flux at the inner side of the SC ($\tilde{x} = \tilde{H}$) is determined solely by diffusion. During the pause between pulses, the migrational component is equal to zero due to a zero electric field. During the pulse, the migrational component also vanishes due to sink conditions [$c(\tilde{x} = \tilde{H}) = 0$]. The instantaneous value of the flux at $\tilde{x} = \tilde{H}$ is determined by the relaxation of the concentration profile, and can be estimated as

$$j_{\tilde{H}} = D\left.\frac{dc}{d\tilde{x}}\right|_{\tilde{x}=\tilde{H}} \approx c_0\left(\frac{D}{t}\right)^{1/2} \qquad (15)$$

Thus, the average flux density at the base of the SC is equal to

$$\bar{j}_{\tilde{H}} = \frac{1}{t_p + t_i}\int_0^{t_p + t_i} j_{\tilde{H}}(t)\,dt \cong 2c_0\left(\frac{D}{t_i}\right)^{1/2} \qquad (16)$$

Equations 14 and 16 give the same result for average flux density because the distance moved by the front during the pulse (vt_p) is equal to the distance during diffusional relaxation ($[D \cdot t_i]^{1/2}$). In other words, because of mass balance considerations, the average flux out of the SC must be equal to the average flux in. Computer calculations of $j_{\tilde{H}}(t)$ and $\bar{j}_{\tilde{H}}$ are illustrated in Fig. 6. The flux was calculated numerically using Eq. 15 (left equality), and the numerical approximation of $C(x, t)$ described above. The sharp increase of the flux during the pulse is related to the rapid spatial advance of the concentration profile, as shown from the curve 7 to the curve 8 in Fig. 5. The

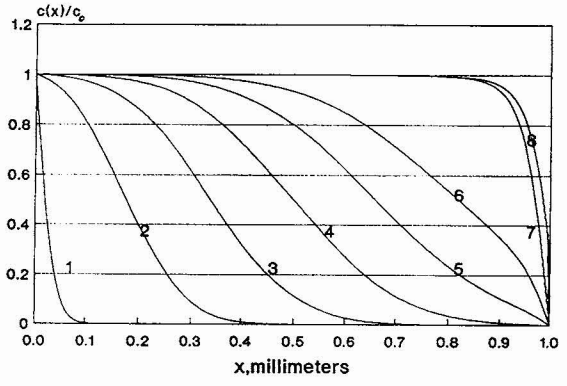

FIGURE 5 The concentration profile $c(x)$ at different moments of time. The numerical solution of the problem on the interval $0 < x < (=1$ mm). Curve 1, 5 s; 2, 50 s; 3, 100 s; 4, 150 s; 5, 200 s; 6, 250 s. Curves 7 and 8 correspond to the pulsations within the space limited by these curves.

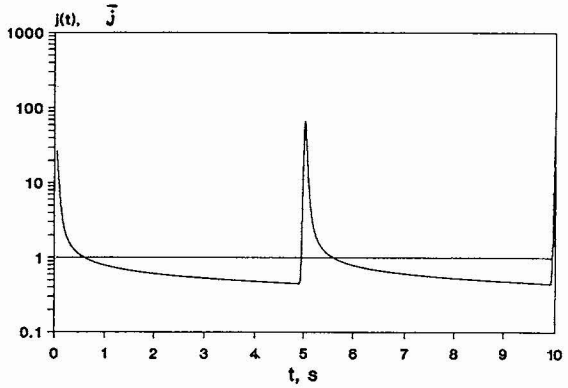

FIGURE 6 The oscillations of the flux density on the outlet side of the SC during electrical treatment in steady state. Numerical solution of the problem with boundary condition $c(\tilde{H}) = 0$.

steep concentration profile at $\tilde{x} = \tilde{H}$ (curve 8) results in a high value for the flux. The transition from curve 8 to curve 7 during the pause between pulses occurs relatively slowly because of diffusional relaxation, as shown in Fig.6.

The average flux density per unit of apparent surface (J) can be written as

$$J = \bar{j} \cdot \pi r^2 N(t) = \bar{j} \cdot f(t) \tag{17}$$

where r is the effective radius of a single pathway and $N(t)$ is the density of pathways, which depends upon $U_s(t)$ and t; $f(t)$ is a fractional area of all pathways. We assume that a number of accessible pathways (N) is equal to the density of pores in the lipid bilayers. The value of $\bar{j}_0$ is defined by the Eq. 14 or 16 and $N(t)$ is a solution of Eq. 5.

Flux relaxation

The relaxation of $J(t)$ after electrotreatment ($t > t_f$) is related to the diffusional relaxation and pore resealing, which can be described by the equation

$$N(t) = N(t_f)\exp\left(\frac{t_f - t}{t_r}\right). \tag{18}$$

The diffusional relaxation can be approximated as

$$j(t) = c_0\left[\frac{D}{t - t_f}\right]^{1/2}. \tag{19}$$

Equation 19 is valid for the time interval when $j(t) > j_{st}$, where $j_{st} = Dc_0/\tilde{H}$. At other times, $j(t) = j_{st}$.

For $J(t)$ we have

$$J(t) = c_0\left[\frac{D}{t - t_f}\right]^{1/2} f(t_f)\exp\left[\frac{t_f - t}{t_r}\right]. \tag{20}$$

Eq. 20 suggests that at short times, fast relaxation is related to a change in the concentration profile within the SC layer. At intermediate times, two effects are superimposed: diffusional relaxation and pore resealing. At longer times, only exponential resealing affects the behavior of $J(t)$.

At the end of electrotreatment ($t = t_f$), the flux density can be written as

$$J(t_f) = \frac{zeD}{kT}\frac{U_s}{\tilde{H}}\frac{t_p}{t_i} c_0 f(t_f). \tag{21}$$

STRAIGHT-THROUGH (LIPID-CORNEOCYTE) MODEL

As was mentioned in Structural Model of Stratum Corneum, in the case of rapid redistribution of ionized particles within each compartment, the mathematical formalism is the same for the lipid and lipid-corneocyte routes. The only difference between the two is in the magnitude of each compartment's accessible hydrophilic volume. For this reason, here we consider these two pathways together.

The characteristic time for the electromigrational filling of the compartment (Fig. 2 *d*) can be estimated as

$$t_{em} \approx \frac{c_0 l \gamma}{J_{em}}, \tag{22}$$

where

$$J_{em} = \frac{zeD}{kT} c_0 E_{av} f. \tag{23}$$

In Eq. 22, γ is the accessible fraction of the compartment's volume and f is the fraction of porated area. In Eq. 23, the time-averaged electric field (E_{av}) in the boundary bilayer region during periodic treatment is

$$E_{av} = \frac{t_p}{t_i} \cdot \frac{U_i}{nd}. \tag{24}$$

The numerical estimation of the filling time (t_{em}) for the calcein flux results discussed above (Prausnitz et al., 1993) gives a value of 0.6 s, assuming $F_w = 10^{-6}$, and $\gamma = 10^{-2}$. These values of f and γ will be justified later from the fitting the theory with experimental data.

The diffusional relaxation time into a compartment is about $t_d \sim l^2/D \sim 10^{-2}$ s, which is small compared with $t_{em} \sim 0.6$ s, suggesting that the concentration c_i within any compartment can be considered homogeneous, yet differing in a stepwise manner from layer to layer in the x direction.

The mass balance equation in this approach is derived in Appendix C and has the form of Eq. C4. This system is convenient for numerical calculation. For analytical considerations, the partial differential Eq. C6 is more suitable.

Concentration profile

Let us rewrite Eq. C6 in the form

$$\frac{\gamma}{f(t)}\frac{\partial c}{\partial t} = \tilde{D}\frac{\partial^2 c}{\partial x^2} - B\frac{\partial c}{\partial x}, \tag{25}$$

where

$$\tilde{D} = D\left(\frac{l}{\tilde{h}}\right); \qquad B = \frac{zeE_{av}D}{kT}, \tag{26}$$

and $\tilde{h}$ is the thickness of boundary layer.

It is useful to introduce renormalized time:

$$\tilde{t} = \int_0^t f(y)\, dy, \tag{27}$$

which then simplifies Eq. 25 to

$$\gamma\frac{\partial c}{\partial \tilde{t}} = \tilde{D}\frac{\partial^2 c}{\partial x^2} - B\frac{\partial c}{\partial x}. \tag{28}$$

After time renormalization, Eq. 28 coincides with Eq. 11, which was solved in Appendices A and B.

When $\tilde{t} < \gamma H/B$, the solution corresponds to the propagation of a concentration profile with the coordinate of the

front equal to $B\tilde{t}/\gamma$. In a real time scale, the front distance (x_{fr}) is described by

$$x_{fr} = \frac{B}{\gamma}\int_0^t f(y)\,dy. \tag{29}$$

In the case of a time-dependent pore area density [$f(t)$], the concentration front propagates with a velocity depending on time:

$$v(t) = \frac{Bf(t)}{\gamma}. \tag{30}$$

The evolution of this concentration profile is illustrated in Fig. 7. It was obtained by the same method as was used for the numerical solution of Eq. 11. The dispersion or spreading of the front is equal to

$$\Delta x_{fr} = \left[\frac{\tilde{D}}{\gamma}\int_0^t f(y)\,dy\right]^{1/2}. \tag{31}$$

When $\tilde{t} > \gamma H/B$, the concentration profile tends to steady-state profile $c_{st}(x)$, which has a form (see Appendix B):

$$c_{st}(x) = \frac{\exp(H\,B/\tilde{D}) - \exp(xB/\tilde{D})}{\exp(H\,B/\tilde{D}) - 1}c_0. \tag{32}$$

It is easy to see that the concentration is practically equal to c_0, when $0 < x < H - \delta H$, $\delta H = B/\tilde{D}$.

Flux density

The flux density $J(x, t)$ has a form

$$J(x, t) = \left[Bc(x, t) - \tilde{D}\frac{\partial c(x, t)}{\partial x}\right]. \tag{33}$$

At $x = 0$

$$J(0, t) \cong Bc_0 f(t)(1 + \exp(-H\,B/\tilde{D})) \cong Bc_0 f(t). \tag{34}$$

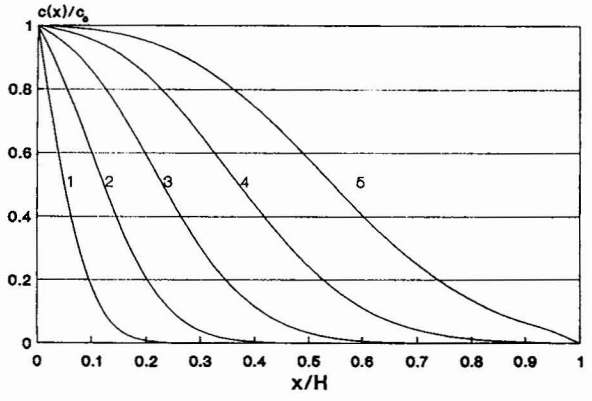

FIGURE 7 The propagation of concentration profile through SC during electrotreatment (s, model). The curves were calculated numerically for $f(t) = f_\infty(1 - \exp(-t/t_f))$. This function $f(t)$ is the solution of Eq. 5 without voltage-divider effect; the values of the parameters $t_f = 1$ h, $f_\infty = 10^{-6}$ were used. 1, after 5 min; 2, after 10 min; 3, after 15 min, 4, after 20 min; 5, after 25 min.

At steady-state, the flux does not depend on x and is equal to

$$J_{st} = \frac{zeD}{kT}\frac{U_1}{nd}\frac{t_p}{t_i}c_0 f(t). \tag{35}$$

This equation is similar to Eq. 21; however, the effective length (nd) is much smaller than in the case of a tortuous pathway. Another important difference between these two cases is the characteristic times of the front propagation. According to Eq. 29, the characteristic time for the straight-through model is equal to

$$\tilde{t}_{fr} = \frac{\gamma H}{B}. \tag{36}$$

In the real time scale, we have the integral equation where the time of front propagation is t_{fr}:

$$\frac{\gamma H}{B} = \int_0^{t_{fr}} f(t)\,dt. \tag{37}$$

The simplest estimation of t_{fr} is

$$t_{fr} \cong \frac{\gamma H}{Bf}. \tag{38}$$

Using Eq. 34, we can rewrite this equation in the form more convenient for a comparison with experimental data:

$$t_{fr} \cong \frac{\gamma H c_0}{J}. \tag{39}$$

Assuming a fractional porosity $f = 10^{-6}$ and $\gamma = 10^{-2}$, then according to Eq. 38, t_{fr} is about 20 min. Using a calcein flux value of about 10^{-7} g/cm^2 h and c_0 of 10 μg/ml (Prausnitz et al., 1993), t_{fr} was determined to be approximately 15 min, in reasonable agreement with the calculated value.

Flux relaxation

We assume that the time of electrotreatment is sufficient to obtain a stationary concentration profile. Eq. 25 describes the concentration profile also in the case where $E = 0$, and with new boundary and initial conditions

$$c(0, t) = c_0 \qquad c(H, t) = 0 \qquad c(x, t_f) = c_{st}(x). \tag{40}$$

The approximations for the flux are as follows:

$$J(\tilde{t}) \cong c_0\left(\frac{\tilde{D}}{\gamma(\tilde{t} - \tilde{t}_f)}\right)^{1/2}, \qquad (\tilde{t} - \tilde{t}_f) < \frac{\gamma H^2}{\tilde{D}}. \tag{41}$$

The flux in real time is

$$J(t) \cong c_0 f(t)\left(\frac{\tilde{D}}{\gamma\int_{t_f}^t f(y)\,dy}\right)^{1/2}. \tag{42}$$

This expression is valid for time smaller than the value t^* defined by the equation

$$\int_{t_f}^{t^*} f(y)\,dy = \frac{\gamma H^2}{\tilde{D}}. \tag{43}$$

For time greater than t^*, the flux density is defined by the equation

$$J = \frac{\tilde{D}\, c_0 f(t)}{H}. \qquad (44)$$

The relaxation of concentration profile is illustrated in Fig. 8. This numerical solution of the Eq. C6 was obtained by the method of Runge-Kutta (Merson's modification).

FITTING OF THE EXPERIMENTAL DATA TO THEORETICAL MODELS

Two kinds of experimental data are suitable for a fitting to the models derived here. They are flux relaxation after electrotreatment and the dependence of the flux at the end of electrotreatment on the voltage. The flux relaxation results following U_s = 90 V electrotreatment are shown in Fig. 9 (*triangles*). These data show the relaxation of calcein flux, which approaches a constant value about 2 h after electrotreatment due to irreversible effects. The data obtained at time less than 2 h after electrotreatment, however, reflect primarily reversible effects. Similar results were obtained at all potentials evaluated, with initial flux value increasing with increased applied voltage.

The experimental data (Prausnitz et al., 1993) were obtained as the average calcein flux over some time interval after electrotreatment. Equations 20 and 42 provide an instantaneous value of the flux. Thus, to compare the experimental data (J_{exp}) with the theoretical results (J_{theor}), it is necessary to integrate Eqs. 20 or 42 over corresponding experimental time intervals (Δt):

$$J_{theor}(t, U_s) = \frac{1}{\Delta t}\int_t^{t+\Delta t} J(z)\, dz. \qquad (45)$$

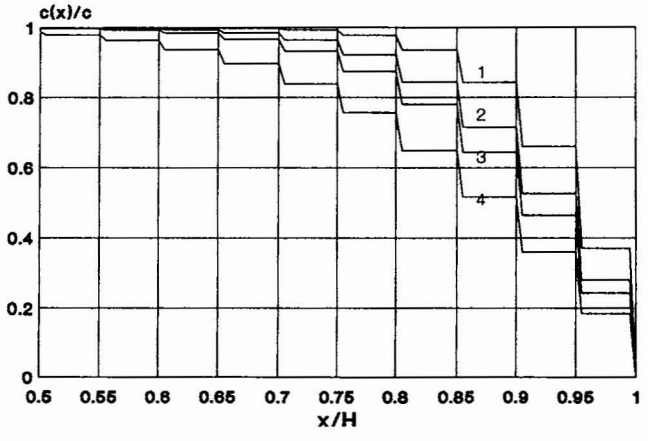

FIGURE 8 The relaxation of concentration profile after electrotreatment (s, model). The curves were calculated numerically for $f(t) = f(t_f)\exp(-t - t_f)/t_r)$ according to Eq. 18, the values of the parameters $f(t_f) = 10^{-6}$, t_r = 1 h were used. 1, 5 min after the end of the treatment; 2, 10 min after; 3, 15 min after. Concentration profiles tend to the curve 4 when $t \to \infty$. It is clear that some amount of substance is trapped within the compartments because of pore resealing.

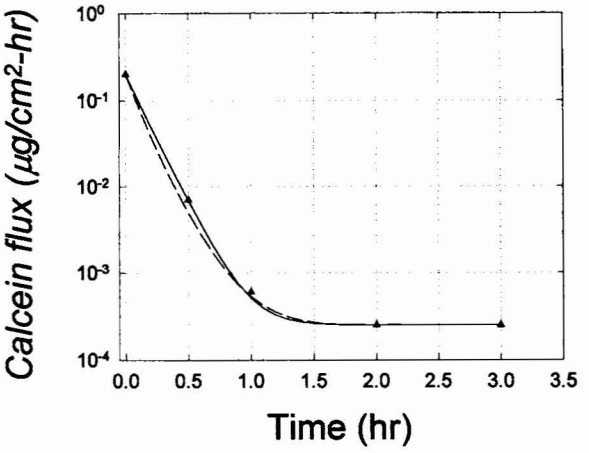

FIGURE 9 Dependence of flux density on time ($t - t_f$) for U_s = 90 V. (*triangles*) Experimental data from Prausnitz et al. (1993). Theoretical curves were plotted with Eq. 20 for tortuous model (——), and Eq. 44 for straight model (- - - -). Fitting parameters are collected in the table.

The best fit made by the method of least-squares for the data obtained after 90 V electrotreatment is shown in Fig. 9 by solid (tortuous model) and dashed (straight-through model) curves. Similar results were seen for all voltages evaluated. The resealing time for the straight-through and tortuous models for all potentials is about 16 min. The close agreement between these two cases is primarily because electropore resealing is common for both models.

The voltage dependence of the flux at the end of electrotreatment is illustrated by the triangles in Fig. 10. These results show that the flux increases by several orders of magnitude in the range of 25 V < U_s < 100 V and then becomes gradually increasing with increased potential.

The analysis of the equivalent scheme from Fig. 4 leads to the Eqs. 9 and 10, which qualitatively explain the experimental results shown in Fig. 10. The quantitative fitting, shown by solid (tortuous route) and dashed (straight-through

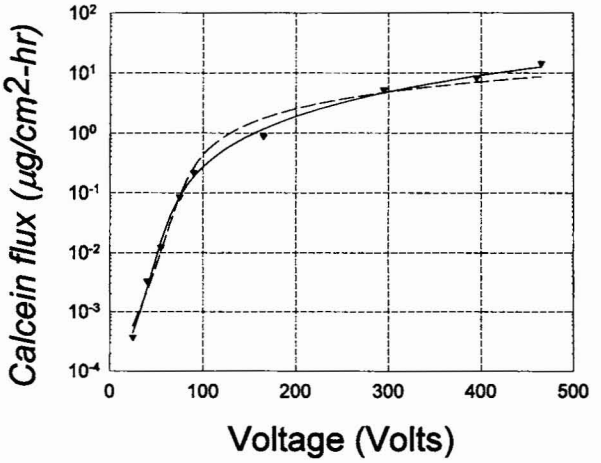

FIGURE 10 Dependence of flux density at $t = t_f$ on voltage. (*triangles*) Experimental data from Prausnitz et al. (1993); theoretical curve was plotted according Eqs. 21 and 37 for tortuous and straight-through models. Fitting parameters are collected in the table.

path) curves in Fig. 10, was done using Eqs. 21 and 35 for the fluxes in the tortuous and straight-through models, respectively, and Eq. 7 for the pore density N as a function of the voltage.

The electroporation parameters ν, a, W^0 were taken from Glaser et al. (1988). For D and c_0, we used the values 10^{-6} cm^2/s and 0.01 M, according to Prausnitz et al. (1993). The corresponding values of α, r, and R_c for both models are considered fitting parameters, and their values are shown in Table 1. The parameter α, estimated from the Eq. 6 with $n = 100$, leads to the value 4.8×10^{-4} V^{-2}, in good agreement with the results in Table 1. The values of inner-compartment resistance $R_c = 2800$ ohms cm^2 (s model) and $R_c = 7200$ ohms cm^2 (t model) are much larger compared with $R_s \sim 400$ ohms cm^2, in agreement with the important assumption of the theory.

The most crucial is fitting parameter (r). The pore radius in the straight-through model, $r_s = 4.0$ Å, seems reasonable. This value is of the same order of magnitude as the molecular radius of calcein. The pore radius in the tortuous model, $r_t = 200$ Å, seems too large even taking into account that it does not represent the radius of the pore in the bilayer, but an effective radius of the pathway that includes inter-bilayer gaps.

From these fitting parameters, the fraction of porated area and pore density were obtained (see Table 2). First, the results show that the porated area increased with increased applied potential for either model, consistent with electroporation results obtained in other lipid systems. The values of f_t, however, are three orders of magnitude larger for the lipid model, because of the longer pathway and weaker effective electric field in this tortuous route. This f_t value ($\sim 10^{-3}$) suggests that 0.1% of the surface is permeable in the lipid model. From the electron microscopic (Elias et al., 1977) and x-ray (Bouwstra et al., 1992) data, the overall fractional area of the inter-bilayer gaps can be estimated to be about 10^{-3}, similar to f_t obtained here. This suggests that in the tortuous (lipid) model, the entire inter-bilayer space should be of sufficient polarity to allow the transport of large, ionized molecules. This conclusion is not consistent with experimental results showing a very low water content of stratum corneum lipids (Potts and Francoeur, 1991).

In the straight-through model, f_s is much smaller so only 10^{-4}% of the surface should be accessible for calcein transport. For the straight-through (lipid-corneocyte) model, the fractional free volume of the reservoirs (γ) was also determined from a fit to the flux-voltage data. The values obtained at all potentials was $\gamma \leq 10^{-2}$ and, in fact, it was not possible to achieve steady state under the experimental conditions

TABLE 1 The values for α, pore radius (r), and resistance of the compartment interior for the s and t models

Model	α (V^{-2})	F (Å)	Rc (ohm cm^2)
s	9.0×10^{-4}	4.0	2800
t	1.3×10^{-4}	200	7200

TABLE 2 Fractional porated area f and pore density N at different voltages for s and t models

U_s (V)	f_s	N_s (cm^{-2})	f_t	N_t (cm^{-2})
50	4.5×10^{-9}	7.9×10^5	2.50×10^{-5}	1.8×10^6
100	2.0×10^{-7}	3.4×10^7	4.0×10^{-4}	3.0×10^7
200	1.0×10^{-6}	1.8×10^8	1.4×10^{-3}	1.0×10^8
500	3.5×10^{-6}	6.2×10^8	4.3×10^{-3}	3.2×10^8

The data in the Table 2 were obtained from fitting parameters shown in Table 1.

evaluated using a value γ of greater than 10^{-2}. As a consequence, in the case of $\gamma > 10^{-2}$, the dependence f_s (U_s) becomes gently sloping. For example, at $\gamma = 10^{-1}$, we get: $f_s(U_s = 55\text{ V}) = 1.3 \times 10^{-6}$; $f_s(U_s = 90\text{ V}) = 3.9 \times 10^{-6}$; $f_s(U_s = 165\text{ V}) = 8.4 \times 10^{-6}$, which is in contradiction with experimental data. Although the corneocytes are full of macromolecules, $\gamma = 10^{-2}$ seems too small. In contrast, this value coincides well with a geometrical estimation of the fractional volume associated with inter-bilayer domain, namely, $\gamma \approx \delta n/H = 5 \times 10^{-3}$. These results suggest that the ion reservoir of this model is more likely associated with polar head groups that form the inter-bilayer hydrophilic domain within SC multilayers.

DISCUSSION

In this paper, several models for the transport of large ionized molecules through the skin are considered. These include transport through the skin appendages such as hair follicles or sweat glands (appendageal route), or through the SC, either entirely within the lipid lamellae bypassing the corneocytes (lipid route), or crossing both the corneocytes and lipid bilayers (lipid-corneocyte route). The relative contribution of each route to the total ion transport depends on the applied voltage. At low applied potential ($U < 1$ V), transport occurs primarily through the appendageal pathway, involving electromigration through these macroscopic ducts. Ultimately, however, the ionized molecule must cross the epithelial cell membrane that lines the bottom of the duct. Preexisting leaks and ion channels in these epithelial cell membranes are sufficient to allow the passage of current, especially in the case of small ions. In the region of intermediate potential ($U \sim 1$ V), experimental results (Kasting and Bowman, 1990a, b) suggest the possible electroporation of epithelial cell membranes within the appendageal pores. As was shown by Prausnitz et al. (1993), calcein flux through human skin increased dramatically when the applied voltage exceeded about 100 V. Bommannan et al. (1993, 1994) showed a significant increase in skin transport of various peptides after the application of a single pulse of a few hundred volts. Similarly, Vanbever et al. (1994) showed enhanced transport of metaprolol through rat skin with pulses exceeding about 100 V. Activation of the appendageal pathway cannot explain this effect, however, because saturation of electroporation in the uni-lamellar epithelial cell membranes must occur at a lower voltage. It is possible, however, that enhanced permeability could result from electrically induced deformation

of sweat glands (Edelberg, 1971). The consideration of this mechanism, however, is beyond the scope of this paper. It is reasonable to consider, therefore, the creation of new pathways at this relatively high voltage due to the electroporation of SC lipids. Although the theory of lipid bilayer has been developed (Abidor et al., 1979; Glaser et al., 1988; Chizmadzhev and Pastushenko, 1988; Freeman et al., 1994), an adequate description of the same phenomenon at the tissue level is absent. For therapeutic applications, it is important to elucidate not only the mechanism of skin electroporation but also its effect on drug transport.

A quantitative theory of electroporative delivery of charged molecules through the skin is presented here, which is based upon a compartment model of the SC consisting of both preexisting and electroinduced hydrophilic pathways. Evidence obtained from a variety of studies (Oh et al., 1993; Potts and Francoeur, 1991) suggests that during transport through skin, ionized molecules must cross lipid bilayers. From electron microscopy and x-ray diffraction results (Holbrook and Odland, 1974; Swartzendruber et al., 1989; Elias et al., 1977; Bouwstra et al., 1992), it can be concluded that these lipids occur in multilamellar structures, found between corneocytes throughout the SC. In addition, capacitance (Oh et al., 1993) and other results suggest that there are on the order of 100 bilayers across the SC. Although there are no data on the "threshold" voltage for the bilayers with lipid composition typical for SC, values near 0.5–1 V are known for several model and cell membranes (Tsong, 1991; Glaser et al., 1988). Thus, it is reasonable to assume that 0.5 V across a single bilayer of the SC, or about 50 V total potential difference across the skin will be sufficient for electroporation of the SC. In the models developed here, these multi-lamellae serve to divide the SC into isolated compartments. During high voltage electrotreatment, pores are induced in these lipid domains and the compartments become connected to form continuous, "open" hydrophilic pathways.

Several alternative versions of the transport model have been developed. In one, the corneocyte is considered impermeable so that transport occurs only within SC lipids. According to this model (the tortuous (lipid) route (designated t in Fig. 2 *a*)), the slow transport process is electromigration along the inter-bilayer hydrophilic pathways between the polar head groups. Pores are then induced in the lipid domains by the applied electric field (see Fig. 2 *a*, *inset*) resulting in a continuous (albeit, highly tortuous) hydrophilic pathway. It is assumed that the electric field has no effect on the geometry or permeability of the inter-bilayer domains, but it is of primary importance for electroinduced permeabilization of the lipid bilayers. In an alternative model (the straight-through (lipid-corneocyte) model (designated s in Fig. 2 *a*)), the hydrophilic space of the SC is considered to consist of ion reservoirs that are connected during electrotreatment by pores induced in lipid bilayers (see Fig. 2 *d*). It is assumed in this model that transport within each reservoir is a fast process relative to electromigration through porated boundary bilayers. Either corneocytes and/or inter-bilayer, hydrophilic domains between these two reservoir models is the accessible hydrophilic volume, which is much greater in the case of the corneocytes.

In the tortuous (lipid) route, electrotreatment serves to permeabilize the lipid, especially boundary bilayers separating the compartments, thereby creating a continuous, "open" hydrophilic pathway. The resultant pathway, which bypasses the corneocytes, is characterized by a high tortuosity, which increases the effective pathway length within the SC. As a consequence of the increased length, the effective electric field is diminished, thereby reducing driving force of migration. The equivalent model is shown in Fig. 2 *c*, where the effective pathway length ($\tilde{H}$) is increased by the tortuosity (β). Using this model, the concentration profile of ionized molecules within the SC was evaluated after electrotreatment conditions, which result in enhanced skin transport. An estimation of the characteristic times for diffusion and migration under these experimental conditions leads to the conclusion that electromigration is the more effective process. In addition, during each pulse the concentration front moves with constant velocity, whereas between pulses diffusional broadening takes place. The evolution of the concentration profile is illustrated in Fig. 5. These results show that under the electrotreatment conditions considered, the front reaches the outlet side of the SC in about 8 min, or after the application of about 100 pulses. Diffusional broadening during this time is relatively small so that the upper 80% of the SC achieves the initial solution concentration c_0. When the electrotreatment is continued for a longer time, a periodic steady pattern is established with oscillations of the concentration profile at the outlet side of the SC. This oscillation is due to alternating electromigration and diffusion. During the application of the pulse, the front becomes very steep, whereas during the pause, it shifts back as a result of diffusional relaxation, which leads to broadening of the profile (see curves 7 and 8 in Fig. 5). It should be mentioned that the boundary condition [$c = 0$ at $x = \tilde{H}$; so called "sink" condition] is very important for this kind of behavior.

In Electroporation of SC Lipid Bilayers, using the tortuous (lipid) model, flux densities on inlet and outlet sides of the SC were considered for a single "open" pathway. Initially, the transport process includes the movement of the concentration front from the outer to inner surface of the SC. During this stage, transport into the SC occurs but efflux is negligible. Ultimately, a periodic steady-state flux (of a single pathway) is established, where at the inlet side of the SC, the flux is migrational and follows $E(t)$, whereas at the outlet side, if "sink" conditions are maintained, the flux includes only a diffusional component (Fig. 5). At steady state, the average influx must equal the average efflux.

In calculating the flux density per unit of apparent surface area, the theory of the reversible electroporation was used to provide a description of the number of pathways as a function of time (Electroporation of SC Lipid Bilayers). We assume that the total density of "open" pathways is equal to the electropore density. The resultant description showed that the

amplitude of the oscillations and the average flux density increases during electrotreatment, but at longer times, it reaches saturation because of both pore relaxation and a decreased voltage drop across the lipid bilayers during electroporation (the "voltage divider" effect). After electrotreatment, flux relaxation occurred because of both diffusional and pore relaxation.

The results were obtained in a simplified model of the SC where the tortuous (lipid) route was considered to be equivalent to a straight pathway of greater length and uniform radius. In reality, the continuous hydrophilic pathway created during electrotreatment is likely to be very nonhomogeneous, and is better described by pathways that have differing lengths and radii. The stochastic properties of these pathways will provide additional (and probably the main) input into broadening of the concentration profile. Nevertheless, the oscillatory nature of flux can be explained by the present simplified model.

In Straight-Through (Lipid Corneocyte) Model, an ion reservoir (lipid-corneocyte) model of the SC hydrophilic space was considered. In this model, equilibration within the hydrophilic domain was considered to be rapid. The hydrophilic domain in principle includes both the inner corneocyte space and inter-bilayer gaps. If the corneocyte envelope is impermeable for large charged particles (for example, calcein), then only the inter-bilayer gaps serve as the ion reservoir. These two cases are considered in the same formalism, except for the differences in the free volume associated with each. During electrotreatment, the reservoirs are connected via pores induced in the SC lipid barriers. The diffusional relaxation time in the compartments is estimated to be about 0.01 s. This value is small compared with the characteristic time of the reservoir filling due to electromigration ($t_{em} \sim 0.6$ s), estimated from typical values of the applied field and the porated area of lipid multilayers that form the main transport barrier. This estimation justifies the assumption that the concentration within each compartment is homogeneous, decreasing in a step-like manner from one compartment to the next with increasing depth into the SC (Fig. 8). The concentration profile for this model also has a form of propagating and broadening front, but its velocity depends on time (Fig. 7). We do not consider the detailed time behavior of the front during periodic electrotreatment, but introduce an equivalent average field and calculate the smoothed response. The time to establish steady state depends on two unknown parameters, the compartment free volume (γ) and porated area (f).

The steady-state flux for the straight-through (lipid-corneocyte) model is described by Eq. 35, which coincides with Eq. 21 for the tortuous (lipid) model. The significant difference between these models is that the electromigration driving force is three orders of magnitude smaller in the lipid model because, due to high tortuosity ($\beta \sim 50$), the effective length is 50-fold greater than H, whereas the effective length (nd) in the straight-through (lipid-corneocyte) model is 40-fold smaller than H. As a result, to obtain the same flux, the porated area must be in three orders of magnitude greater in the tortuous versus the straight-through model.

In Fitting of the Experimental Data to Theoretical Models, the models described here were used to fit the experimental results. From flux relaxation data (Fig. 9), a characteristic time of about 16 min was found for both transport mechanisms. This time was attributed to pore resealing after electroporation. We cannot exclude, however, the possible role of retention within the epidermis.

The most informative data to choose among the different models proposed are the voltage dependencies of the flux at the end of electrotreatment (Fig. 10). These results show that the flux increases by several orders of magnitude in the range $25\ \text{V} \leq U_s \leq 100\ \text{V}$ and with relatively little further increase at higher potential. This kind of flux behavior is described by equivalent scheme in Fig. 4. The current-voltage characteristics of the system also include the steep and smooth regions, albeit in a different range of voltage. The strong dependence takes place at the potentials where R_x is a nonlinear function of voltage. From the impedance measurements (Prausnitz et al., 1993), it is clear that this effect occurs at voltages smaller than $U \cong 50$ V. After that, the first voltage divider between R_b and R_s is practically linear, and U_s can be considered known voltage superimposed on the skin. For this reason, in Fig. 10 the flux is plotted as a function of U_s, which depends on R_x.

The theoretical curves take into account a voltage divider effect (see Eq. 4), so that with increasing applied voltage and, hence, increasing electroporation, the resistance R_ℓ and potential drop U_ℓ decrease. As a consequence of the decreased U_ℓ, further electroporation is limited. Similar results have been obtained for the electroporative calcein uptake by cells (Prausnitz et al., 1993; Wang et al., 1992).

Although the goodness-of-fit invariably increases with the number of parameters, the parameters chosen here are consistent with electroporation theory and the skin's structure (Figs. 1 and 2) and the equivalent electrical circuit (Fig. 4). Moreover, although general, the models predict the unique nonlinear flux-voltage behavior seen experimentally. Further, experimental work is required to understand the molecular details and thereby refine the model.

The most crucial fitting parameter in our procedure is pore radius (r). The large pore radius ($r_t \sim 200$ Å) and fractional area ($f_t \sim 10^{-3}$) obtained for the tortuous (lipid) model relative to the values obtained for the straight-through model ($r_s \sim 4$ Å, $f_s \sim 10^{-6}$) suggests that the latter is a more realistic description of electroinduced transport of ionized species through the skin. In addition, the small value of the fractional free volume ($\gamma \leq 10^{-2}$) indicates that inter-bilayer domains are more probable candidates for calcein reservoirs. The results presented here suggest that enhanced transport through human skin after high voltage electrotreatment can be explained by electroporation within SC lipids. Definitive choice between tortuous and straight-through transport models awaits further experimental results.

We are very much obliged to B. Bommannan, V. Bose, P. Kuzmin, and M. Prausnitz for fruitful discussions. We are grateful to Loretta Linderman who did the hard work of preparing this manuscript for publication.
The support of Cygnus Therapeutic Systems, National Institutes of Health grant ES06010, and the Ministry of Science of Russia is acknowledged.

APPENDIX A

Electrodiffusion in a semi-infinite medium

We will analyze the solution of the equation

$$\frac{\partial c}{\partial t} = D\frac{\partial^2 c}{\partial x^2} - \frac{zeD\tilde{E}}{kT}\frac{\partial c}{\partial x}, \tag{A1}$$

with boundary condition

$$c(0, t) = c_0, \qquad t > 0 \tag{A2}$$

and initial condition

$$c(x, 0) = 0, \qquad x > 0. \tag{A3}$$

Let us write Eq. A1 in the following form:

$$\frac{\partial c}{\partial t} = D\frac{\partial^2 c}{\partial x^2} - AD\frac{\partial c}{\partial x}; \qquad A = \frac{ze\tilde{E}}{kT}.$$

Let us introduce the new function:

$$g(x, t) = c(x, t) - c_0.$$

This function satisfies Eq. A1 and the conditions

$$g(0, t) = 0; \qquad g(x, 0) = -c_0.$$

The solution can be presented in the form

$$g(x, t) = \tilde{g}(x, t)\exp(\lambda x + \mu t). \tag{A4}$$

Our aim is to reduce Eq. A1 to a simpler form that does not contain a migration term. Substituting (A4) into (A1), we get

$$D\frac{\partial^2 \tilde{g}}{\partial x^2} + D\frac{\partial \tilde{g}}{\partial x}(2\lambda - A) + \tilde{g}\cdot(\lambda^2 D - AD\lambda - \mu) = \frac{\partial \tilde{g}}{\partial t}. \tag{A5}$$

Taking $\lambda = A/2$ and $\mu = -A^2D/4$, we obtain

$$D\frac{\partial^2 \tilde{g}}{\partial x^2} = \frac{\partial \tilde{g}}{\partial t} \tag{A6}$$

$$\tilde{g}(x, 0) = -c_0\exp\left(-\frac{Ax}{2}\right) \tag{A7}$$

$$\tilde{g}(0, t) = 0, \qquad t > 0. \tag{A8}$$

The solution of (A6)–(A8) may be written as

$$c(x, t) = c_0 erf\left[\frac{ze\tilde{E}t - xkT}{kT\cdot(2Dt)^{1/2}}\right] + c_0\exp\left(\frac{ze\tilde{E}x}{kT}\right)\left[1 - erf\left(\frac{ze\tilde{E}Dt + xkT}{kT\cdot(2Dt)^{1/2}}\right)\right], \tag{A9}$$

where

$$erf(y) = (2\pi)^{-1/2}\cdot\int_{-\infty}^{y}\exp\left(-\frac{z^2}{2}\right)dz.$$

This solution corresponds to propagation of concentrational front with velocity equal to $ezD^{\tilde{E}}/kT$ and simultaneous broadening of this front due to diffusion with characteristic length of the order of $(Dt)^{1/2}$.

APPENDIX B

Electrodiffusion in the layer $0 < x < \tilde{H}$

Let us consider the electrodiffusion equation with the appropriate boundary and initial conditions:

$$\frac{\partial c}{\partial t} = D\frac{\partial^2 c}{\partial x^2} - \frac{zeD\tilde{E}}{kT}\frac{\partial c}{\partial x}$$

$$c(0, t) = c_0, \qquad c(\tilde{H}, t) = 0, \qquad t > 0 \tag{B1}$$

$$c(x, 0) = 0, \qquad 0 < x < \tilde{H}.$$

We shall consider first of all the stationary problem:

$$0 = D\frac{\partial^2 c_{st}}{\partial x^2} - AD\frac{\partial c_{st}}{\partial x} \qquad c_{st}(0) = c_0 \quad c_{st}(\tilde{H}) = 0, \tag{B2}$$

where

$$A = \frac{ze\tilde{E}}{kT}.$$

The solution of (B2) can be written in the form

$$c_{st}(x) = c_0\frac{\exp(A\tilde{H}) - \exp(Ax)}{\exp(A\tilde{H}) - 1}. \tag{B3}$$

Let

$$c(x, t) = c_{st}(x) + g(x, t), \tag{B4}$$

Then taking $g(x, t)$ in the form

$$g(x, t) = \tilde{g}(x, t)\exp(\lambda x + \mu t), \tag{B5}$$

where

$$\lambda = A/2; \qquad \mu = -A^2D/4.$$

we get

$$D\frac{\partial^2 \tilde{g}}{\partial x^2} = \frac{\partial \tilde{g}}{\partial t} \qquad \tilde{g}(x, 0) = -g(x, 0)\exp\left(-\frac{Ax}{2}\right)$$
$$\tilde{g}(0, t) = g(\tilde{H}, t) = 0. \tag{B6}$$

Using the Green function for the boundary problem (B6), its solution can be presented in the form

$$g(x, t) = -\frac{\exp(Ax/2 - A^2Dt/4)}{(4\pi D\,t)^{1/2}}\cdot\int_0^{\tilde{H}}\sum_{k=-\infty}^{\infty}\left[\exp\left\{-\frac{(x - 2k\tilde{H} - x')^2}{4Dt}\right\} - \exp\left\{-\frac{(x - 2k\tilde{H} + x')^2}{4Dt}\right\}\right]\exp\left(-\frac{Ax'}{2}\right)c_{st}(x')\,dx'. \tag{B7}$$

for the case of a strong electric field $A\tilde{H} \gg 1$ and for $t \cong \tilde{H}/AD$, with rather good accuracy, we may leave only three terms in the series in (B7) and obtain an approximate solution:

$$g(x, t) = -\frac{\exp(Ax/2 - A^2Dt/4)}{(4\pi Dt)^{1/2}}\cdot\int_0^{\tilde{H}}\left[\exp\left\{-\frac{(x - x')^2}{4Dt}\right\} - \exp\left\{-\frac{(x + x')^2}{4Dt}\right\} - \exp\left\{-\frac{(x - 2\tilde{H} + x')^2}{4Dt}\right\}\right]\exp\left(-\frac{Ax'}{2}\right)c_{st}(x')\,dx'. \tag{B8}$$

The resulting $c(x, t)$ behavior is shown in Fig. 5 for several moments of time.

It is seen that the $c(x,t)$ profile propagates from $x = 0$ to $x = \tilde{H}$ with simultaneous broadening and for $t \gg \tilde{H}/v$ with

$$v = \frac{ze\tilde{E}D}{kT}$$

tends to the stationary profile described by Eq. B3.

APPENDIX C

The equations for the straight-through model

According to the estimations of Eqs. 22–24, the concentration and electric potential in each are homogeneous. This means that all gradients are located at the boundary lipid bilayers and the concentration differs in a stepwise manner from layer to layer in the x direction (Fig. 8). Let us consider the mass balance in the compartment number (i). The influx density of the species from the compartment $(i-1)$ consists of diffusional and migrational components:

$$J_{inf} = D\frac{C_{i-1} - C_i}{\tilde{h}} f(t) + \frac{zeE_{av}D}{kT} f(t)c_{i-1}, \qquad (C1)$$

where $\tilde{h}$ is the thickness of boundary layer and $f(t)$ characterizes the accessible (porated) part of the interface. The corresponding equation for the efflux can be written as

$$J_{eff} = D\frac{C_i - C_{i+1}}{\tilde{h}} f(t) + \frac{zeE_{av}D}{kT} f(t)c_i. \qquad (C2)$$

The mass balance equation has the usual form:

$$\ell\gamma\frac{dc_i}{dt} = J_{inf} - J_{eff} \qquad (C3)$$

or

$$\frac{\gamma}{f(t)}\frac{dc_i}{dt} = \frac{D}{\ell}\left[\frac{(c_{i-1} - c_i)}{\tilde{h}} - \frac{(c_i - c_{i+1})}{\tilde{h}}\right] + \frac{zeE_{av}D}{kT\ell}(c_{i-1} - C_i). \qquad (C4)$$

Here (ℓ) practically corresponds to the thickness of the compartment because $h/\ell \ll 1$. This system with $1 \le i \le n_c$, where n_c is the number of corneocytes in sequence, can be solved numerically. However, there exists a good analytical approximation using a smooth function $c(x,t)$ that satisfies the partial differential equation. Considering $\tilde{h}$ as infinitesimally small, $\tilde{h} = \Delta\bar{x}$, in the limit $\Delta\bar{x}\to 0$ (C4) can be expressed as the differential equation

$$\frac{\gamma}{f(t)}\frac{\partial c(\bar{x},t)}{\partial t} = \frac{D\tilde{h}}{\ell}\frac{\partial^2 c(\bar{x},t)}{\partial\bar{x}^2} - \frac{zeE_{av}D\tilde{h}}{kT\ell}\frac{\partial c(\bar{x},t)}{\partial\bar{x}}, \qquad (C5)$$

where $0 < \bar{x} < n_c\tilde{h}$. It is more convenient to introduce the coordinate $x = \bar{x}H/n_ch$, which is restricted by the limits $0 < x < H$ and rewrite the Eq. C5 in the form

$$\frac{\gamma}{f(t)}\frac{\partial c(x,t)}{\partial t} = \frac{D\,l}{\tilde{h}}\frac{\partial^2 c(x,t)}{\partial x^2} - \frac{zeE_{av}D}{kT}\frac{\partial c(x,t)}{\partial x}. \qquad (C6)$$

The boundary and initial conditions for this equation have a form

$$c(0,t) = c_0; \qquad c(H,t) = 0; \qquad c(x,0) = 0. \qquad (C7)$$

REFERENCES

Abidor, I. G., V. B. Arakelyan, L. V. Chernomordik, Y. A. Chizmadzhev, V. F. Pastushenko, and M. R. Tarasevich. 1979. Electric breakdown of bilayer membranes: I. The main experimental facts and their qualitative discussion. *Bioelectrochem. Bioenerg.* 6:37–52.

Benz, R., F. Beckers, and U. Zimmermann. 1979. Reversible electrical breakdown of lipid bilayer membranes: a charge-pulse relaxation study. *J. Membr. Biol.* 48:181–204.

Bommannan, D., L. Leung, J. Tamada, J. Sharifi, and R. Potts. 1993. Transdermal drug delivery of luteinizing hormone releasing hormone: comparison between electroporation and iontophoresis in vitro. *Proc. Intl. Symp. Control Rel. Bioact. Mat.* 20:97–98.

Bommannan, D., J. Tamada, L. Leung, and R. Potts. 1994. Effect of electroporation on transdermal iontophoretic delivery of luteinizing hormone releasing hormone (LHRH) in vitro. *Pharmaceut. Res.* 11:1809–1814.

Bouwstra, J. A., G. S. Gooris, M. A. Salonons-de Vries, J. A. van der Spek, and W. Bras. 1992. Structure of human stratum corneum as a function of temperature and hydration: a wide-angle x-ray diffraction study. *Int. J. Pharmaceut.* 84:205–216.

Burnette, R. R. 1989. Iontophoresis. *In* Transdermal Drug Delivery: Developmental Issues and Research Initiatives. J. Hadgraft and R. H. Guy, editors. 247–291.

Chang, D. C., B. M. Chassy, J. A. Saunders, and A. E. Sowers, editors. 1992. Guide to Electroporation and Electrofusion. Academic Press, New York. 581 pp.

Chizmadzhev, Y. A., and V. P. Pastushenko. 1988. Theory of electrical breakdown of planar lipid bilayers. *In* Thin Liquid Films. J. B. Ivanol, editor. Marcel-Dekker, Basel, Switzerland. 1059–1120.

Cullander, C. 1992. What are the pathways of iontophoretic current flow through mammalian skin? *Adv. Drug Del. Rev.* 9:19–135.

Cullander, C., and R. H. Guy. 1991. Sites of iontophoretic current flow into the skin: identification and characterization with the vibrating probe electrode. *J. Invest. Dermatol.* 97:55–64.

DeNuzzio, J. D., and B. Berner. 1990. Electrochemical and iontophoretic studies of human skin. *J. Controlled Release* 11:105–112.

Dinh, S. M., C.-W. Luo, and B. Berner. 1993. Upper and lower limits of human skin electrical resistance in iontophoresis. *AICHE J.* 39: 2011–2018.

Edelberg, R. 1971. Electrical properties of skin. *In* Biophysical Properties of the Skin. H. R. Elden, editor. John Wiley & Sons, New York. 513–550.

Elias, P. 1983. Epidermal lipids, barrier function and desquamation. *J. Invest. Dermatol.* 80(Suppl.):44s–49s.

Elias, P. M., N. S. McNut, and D. S. Friend. 1977. Membrane alterations during cornification of mammalian squameous epithelia: a freeze-fracture, tracer and thin-section study. *Anat. Rec.* 189:577–599.

Freeman, S. C., M. A. Wang, and J. C. Weaver. 1994. Theory of electroporation of planar bilayer membranes: predictions of the aqueous area, changes in capacitance and pore-pore separation. *Biophys. J.* 67:42–56.

Glaser, R. W., S. L. Leikin, L. V. Chernomordik, V. F Pastushenko, and A. I. Sokirko. 1988. Reversible electrical breakdown of lipid bilayers: formation and evolution of pores. *Biochim. Biophys. Acta.* 940:275–287.

Grimnes, S. 1983. Dielectric breakdown of human skin in vivo. *Med. Biol. Eng. Comp.* 21:379–381.

Holbrook, K. A., and G. F. Odland. 1974. Regional differences in the thickness (cell layers) of the human stratum corneum: an ultrastructural analysis. *J. Invest. Dermatol.* 62:415–422.

Kasting, G. G., and L. A. Bowman. 1990a. DC electrical properties of frozen, excised human skin. *Pharmacol. Res.* 7:134–143.

Kasting, G. G., and L. A. Bowman. 1990b. Electrical analysis of fresh excised human skin: a comparison with frozen skin. *Pharmacol. Res.* 7:1141–1146.

Kinosita, K., Jr., I. Ashikawa, N. Saita, H. Yoshimura, H. Itoh, H. Nagayama, and A. Ikegami. 1988. Electroporation of cell membrane visualized under a pulsed-laser fluorescence microscope. *Biophys. J.* 53:1015–1019.

Kinosita, K., Jr., and T. Y. Tsong. 1977. Formation and resealing of pores of controlled sizes in human erythrocyte membrane. *Nature.* 268:438–441.

Klenchin, V. A., S. I. Sukharev, S. M. Serov, L. V. Chernomordik, and Y. A. Chizmadzhev. 1991. Electrically induced DNA uptake by cells is a fast process involving DNA electrophoresis. *Biophys. J.* 60:804–811.

Lakshminarayanaiah, N. 1984. Equations of Membrane Biophysics. Academic Press, New York. 320 pp.

Madison, K. D., D. C. Swartzendruber, P. W. Wertz, and D. T. Downing. 1987. Presence of intact intercellular lipid lamellae in the upper layers of the stratum corneum. *J. Invest. Dermatol.* 88:714–718.

Michaels, A. S., S. K. Chandrasekaran, and J. E. Shaw. 1975. Drug permeation through human skin: theory and in vitro experimental measurements. *AICHE J.* 21:985–996.

Mir, L. M., S. Orlowski, J. Belehradek, and C. Paoletti. 1991. In vivo potentiation of the bleomycin cytotoxicity by local electric pulses. *Eur. J. Cancer.* 27:68–72.

Monteiro-Riviere, N. A., A. O. Inman, and J. E. Riviere. 1994. Identification of the pathway of iontophoretic drug delivery: light and ultrastructure studies using mercuric chloride in pigs. *Pharmacol. Res.* 11:251–256.

Neumann, E., and K. Rosenheck. 1972. Permeability changes induced by electric impulses in vesicular membranes. *J. Membr. Biol.* 10:279–290.

Neumann, E., A. Sowers, and C. Jordan, editors. 1989. Electroporation and Electrofusion in Cell Biology. Plenum Press, New York. 436 pp.

Odland, G. F. 1983. Structure of the skin. *In* Biochemistry and Physiology of the Skin. L. A. Goldsmith, editor. Oxford University Press, Oxford. 3–63.

Oh, S. Y., L. Leung, D. Bommannan, R. H. Guy, and R. O. Potts. 1993. Effect of current, ionic strength and temperature on the electrical properties of skin. *J. Controlled Release.* 9:137–176.

Orlowski, S., and L. M. Mir. 1993. Cell electropermeabilization: a new tool for biochemical and pharmacological studies. *Biochim. Biophys. Acta.* 1154:51–63.

Pearson, C. E., 1988. Handbook of Applied Mathematics. Van Nostrand Reinhold Company. 498–499.

Potts, R. O. 1989. Physical characterization of the stratum corneum: the relationship of mechanical and barrier properties to lipid and protein structure. *In* Transdermal Drug Delivery: Developmental Issues and Research Initiatives. J. Hadgraft and R. H. Guy, editors. Marcel-Dekker, New York. 247–291.

Potts, R. O., and M. L. Francoeur. 1991. The influence of stratum corneum morphology on water permeability. *J. Invest. Dermatol.* 96:495–499.

Potts, R. O., and R. H. Guy. 1992. Predicting skin permeability. *Pharmacol. Res.* 96:495–499.

Potts, R. O., R. H. Guy, and M. L. Francoeur. 1992. Routes of ionic permeability through mammalian skin. *Solid State Ionics.* 53–56:165–169.

Prausnitz, M. R., V. G. Bose, R. Langer, and J. C. Weaver. 1993. Electroporation of mammalian skin: a mechanism to enhance transdermal drug delivery. *Proc. Natl. Acad. Sci. USA.* 90:10504–10508.

Prausnitz, M. R., B. S. Lau, C. D. Milano, R. Langer, and J. C. Weaver. 1993. A quantitative study of electroporation showing a plateau in net molecular transport. *Biophys. J.* 65:414–422.

Scheuplein, R. J., and R. L. Bronaugh. 1983. Percutaneous absorption. *In* Biochemistry and Physiology of the Skin. L. A. Goldsmith, editor. Oxford University Press, Oxford. 1255–1295.

Scott, E. R., A. I. Laplaza, H. S. White, and J. B. Phipps. 1993. Transport of ionic species in skin: contribution of pores to the overall skin conductance. *Pharmacol. Res.* 10:1699–1709.

Sukharev, S. I., V. A. Klenchin, S. M. Serov, L. V. Chernomordik, Y. A. Chizmadzhev. 1992. Electroporation and electrophoretic DNA transfer into cells. *Biophys. J.* 63:1320–1327.

Swartzendruber, D. C., P. W. Wertz, D. J. Kitko, K. C. Madison, and D. T. Downing. 1989. Molecular models of the intercellular lipid lamellae in mammalian stratum corneum. *J. Invest. Dermatol.* 92: 251–257.

Swartzendruber, D. C., P. W. Wertz, K. C. Madison, and D. T. Downing. 1987. Evidence that the corneocyte has a chemically bound lipid envelope. *J. Invest. Dermatol.* 88:709–713.

Titomirov, A. V., S. Sukharev, and E. Kistoanova. 1991. In vivo electroporation and stable transformation of skin cells of newborn mice by plasmid DNA. *Biochim. Biophys. Acta.* 1088:131–134.

Tsong, T. Y. 1991. Electroporation of cell membranes. *Biophys. J.* 60: 297–306.

Vanbever, R., N. Lecouturier, and V. Preat. 1994. Transdermal delivery of metoprolol by electroporation. *Pharmacol. Res.* 11:1660–1665.

Wang, M. A., S. A. Freeman, V. G. Bose, S. Dyer, and J. C. Weaver. 1992. Theoretical modeling of electroporation: electrical behavior and molecular transport. *In* Electricity and Magnetism in Biology and Medicine. M. Blank, editor. San Francisco Press. 138–140.

Weaver, J. C. 1993. Electroporation: a general phenomenon for manipulating cells and tissue. *J. Cell. Biochem.* 51:426–435.

Weaver, J. C., and A. Barnett. 1992. Progress towards a theoretical model of electroporation mechanism: membrane electrical behavior and molecular transport. *In* Guide to Electroporation and Electrofusion. D. C. Chang, B. M. Chassy, J. A. Saunders, and A. E. Sowers, editors. Academic Press, New York. 91–117.

Xie, T.-D., and T. Y. Tsong. 1990. Study of mechanisms of electric field-induced DNA transfection. II. transfection by low amplitude, low frequency alternating electric fields. *Biophys. J.* 58:897–903.